Journal of Materials Chemistry B

PAPER

View Article Online
View Journal | View Issue

Cite this: J. Mater. Chem. B, 2014, 2, 2233

Iridium oxide nanoparticle induced dual catalytic/inhibition based detection of phenol and pesticide compounds†

Carmen C. Mayorga-Martinez,‡[a] Flavio Pino,‡[a] Sevinc Kurbanoglu,‡[ab] Lourdes Rivas,[a] Sibel A. Ozkan[b] and Arben Merkoçi*[ac]

Received 11th December 2013
Accepted 28th January 2014

DOI: 10.1039/c3tb21765e

www.rsc.org/MaterialsB

Environmental pollution control technology has a great demand for detection systems, particularly for pesticides and phenolic compounds. Moreover, analytical systems are highly required for the dual detection of different pollutants using the same platform. In that direction, a new, reliable, easy to use and disposable biosensor for the detection of catechol and chlorpyrifos is proposed. The designed biosensor with synergic properties between the high conductivity of iridium oxide nanoparticles, low-cost screen printed electrodes and the efficiency of tyrosinase shows broad linearity ranges for catechol and chlorpyrifos detection. Using this biosensor, very low limits of detection for catechol (0.08 μM) and chlorpyrifos (0.003 μM) are observed and recoveries of spiked tap and river water samples have also been studied showing very good recoveries.

Introduction

The detection of polluting compounds is a major concern for health and environmental government institutions. Among all pollutant compounds, organophosphate pesticide (OP) and phenol compounds are the most toxic and dangerous ones for human beings.[1,2] It is well known that pesticide and phenol compounds possess highly acute toxicity. For instance, chlorpyrifos (CPF), one of the most widely used OPs, interferes with brain development in part due to alterations in the activity of transcription factors involved in the basal machinery of cell replication and differentiation,[3] and phenol is a potential human carcinogen and is of considerable health concern, even at low levels.[4]

Pesticides are extensively used in farming and for domestic purposes.[5] Phenol compounds have limited use in industrial processes for different purposes.[6] In fact, every day these compounds are easily released in different water systems affecting the ecosystem.

Nowadays, the detection of pesticides and phenol compounds is performed using large and expensive automated analysers such as liquid chromatography coupled with mass spectrometry[7,8] and high pressure liquid chromatography.[9,10] These techniques reach low limits of detection and have high reproducibility, but they involve extraction of large volumes of water, require extensive purification and expensive equipment. Therefore, there is a high demand to obtain simple analytical devices and related nanomaterials for the detection of the mentioned hazardous compounds in environment and health related samples. The main requirements of the future detection systems are to be cheap, reliable, easy to use and disposable. At the same time, it would be necessary to have devices that can detect different families of pollutants.

Currently different approaches for the detection of pesticides, including immunoassay[11] and enzymatic activity,[12] have been developed. Enzymatic biosensors are the most reliable for this type of analysis due to their simplicity, efficiency and their easy usage. In fact, numerous biosensors using inhibition-based enzymatic systems, in particular those based on the inhibition of acetyl cholinesterase (AChE),[13,14] have been reported. Furthermore, tyrosinase (Tyr) has been used for phenolic compound detection, and based on the inhibition of this enzyme some pesticide detections have been reported.[15,16]

The advantage of the Tyr based electrochemical biosensor is its achieved selectivity due to the fact that the effect of interfering species such as other electroactive compounds is low given its low working potential (−0.2 V or less)[17–19] in comparison to AChE and free mediator based biosystems that mostly work at 0.6 V.[20]

Meanwhile, the need for a disposable analytical platform could be reached through the use of micro-transducers like screen printed carbon electrodes (SPCEs). In fact in the last

[a]Nanobioelectronics & Biosensors Group, ICN2-Institut Catala de Nanociencia i Nanotecnologia, Campus UAB, 08193, Bellaterra, Barcelona, Spain. E-mail: arben.merkoci@icn.cat

[b]Ankara University, Faculty of Pharmacy, Department of Analytical Chemistry, 06100, Tandogan, Ankara, Turkey

[c]ICREA, Barcelona, Catalonia, Spain

† Electronic supplementary information (ESI) available. See DOI: 10.1039/c3tb21765e

‡ C. C. M.-M., F. P. and S. K. contributed equally to this work.

twenty years, the application of these devices for *in situ* and user-friendly measurements has significantly increased. The key factor in an enzymatic micro-device platform is the immobilization procedure of the enzyme. This process is usually performed in different ways; adsorption, entrapment and cross-linking are the most reported. The main objective of the enzyme immobilization alternatives has always been the increase of the biosensor stability and its reproducibility, fouling of the working electrode surface being the most important drawback to overcome.[21,22]

The explosion in nanomaterials research, especially nanoparticles, has also influenced the research in the field of enzymatic biosensors.[23,24] The connection of enzymatic systems with nanoparticles has a high impact on improving the performance of the platform used for detection of toxic compounds. This is due to the unique, chemical, physical and electronic properties at nanoscale possessed by nanoparticles (normally in the range of 1–100 nm).[25,26] Iridium oxide (IrOx) films have been used in biosensors as electrodes (enzymes can be immobilized) due to their high conductivity.[27] Furthermore, IrOx nanoparticles possess useful electronic and conductivity switching properties which make them highly attractive for biosensor development as well.[28]

In the present study, an enzymatic biosensor for dual detection of two different pollutants, catechol (a phenol derivative) and chlorpyrifos (an organophosphate pesticide) is proposed. Such sensing is achieved through a SPCE modified with IrOx NPs and tyrosinase. The proposed biosensor reports improvement in the limit of detection (0.08 μM) and sensitivity for catechol compared to previously reported biosensors. This biosensor shows also a low limit of detection (0.003 μM) for CPF while being used in a tyrosinase inhibition mode operation. Finally the efficiency of this biosensor for real applications in CPF detection in river and tap water was also explored showing great possibilities for future application as a low cost platform for pesticide detection.

Experimental

Materials and apparatus

Electrochemical experiments were performed using an electrochemical analyzer Autolab 20 (Eco-Chemie, The Netherlands) which was connected to a personal computer using a software package GPS 4.9 (General Purpose Electrochemical System). Impedance measurements were performed by using an Autolab302 potentiostat/galvanostat/frequency-response analyzer PGST30, controlled by GPES/FRA Version 4.9. Scanning electrochemical microscopy (SEM) images were acquired using a field emission-scanning electron microscope (Merlin, Carl Zeiss) and transmission electron microscope (TEM) images were taken with a JEM-2011(Jeol,Ltd., Japan). A thermoshaker TS1 (Biometra) was used to stir the samples during the inhibition process operating at a controlled temperature of 37.5 °C and shaking at 350 rpm. Homemade screen printed carbon electrodes (SPCEs) were used as electrochemical transducers, which are constituted by three electrodes in a single strip: a carbon working electrode with a diameter of 3 mm, an Ag/AgCl reference electrode and a carbon counter electrode.

Reagents and solutions

Tyrosinase from mushroom (≥1000 unit per mg), bovine serum albumin (BSA), glutaraldehyde (GA, 25%), chlorpyrifos and catechol were purchased from Sigma-Aldrich (St. Louis, MO). For the synthesis of iridium oxide nanoparticles, potassium hexachloroiridate(IV) and sodium hydrogencitrate were purchased from Sigma-Aldrich (St. Louis, MO). Milli-Q water was obtained from a purification system and all solutions were prepared with ultra-pure water from a Millipore-MilliQ system. All reagents and other inorganic chemicals were supplied by Sigma-Aldrich or Fluka, unless otherwise stated.

Synthesis of iridium oxide nanoparticles

Iridium oxide nanoparticles were prepared according to the previously reported procedure.[29] Potassium hexachloroiridate(IV) 2.6×10^{-5} M solution was mixed with sodium hydrogencitrate 1.6×10^{-2} M solution. The pH of the red-brown solution was adjusted to 7.5 with a 0.25 M NaOH solution and then refluxed in an oil bath with constant stirring for 30 min. As the mixture cooled to room temperature, the pH was again adjusted to 7.5 with refluxing for 30 min. This procedure was repeated until the pH reached a constant value of 7.5. Finally the solution was refluxed for a further 2 h with oxygen bubbling. At the end of this step, a deep blue solution of IrOx nanoparticles was obtained. The solution was stored in a glass-stoppered flask and at 4 °C when not in use.

Preparation and modification of screen printed electrodes

Screen printed electrodes were fabricated by sequential deposition of a graphite ink, Ag/AgCl ink and insulating ink on a polyester substrate. The polyester substrate was dried at 120 °C for 45 min (graphite) and 30 min (Ag/AgCl and insulating) after the deposition of each layer. Before modification, SPCEs were activated at 3 μA for 120 s in 0.1 M H_2SO_4. A 5 μL solution of IrOx NPs suspension was dropped onto the working surface of SPCE. 0.25% of glutaraldehyde (GA) was prepared in ultra-pure water and from this solution 5 μL was dropped onto the SPCE/IrOx surface. 2 μL of the solution of Tyr (1 mg per 50 μL) in 5% BSA (1 : 1) was dropped onto the SPCE/IrOx/GA surface. Tyr and BSA solutions were prepared in 0.1 M phosphate buffer at pH 6.5. In between all steps, electrodes were dried at 37.5 °C for 30 min.

Electrochemical measurements

The surface characterization of the modified electrodes was performed by electrochemical impedance spectroscopy (EIS) studies in 1 mM $[Fe(CN)_6]^{3-/4-}$ with 0.1 M KCl as redox probe. A sinusoidal potential modulation of ±50 mV amplitude in the 0.1 Hz to 100 kHz frequency range, with a logarithmic scale of 10 points per decade, was superimposed onto the formal potential of the redox couple, $[Fe(CN)_6]^{3-/4-}$ (0.24 V *vs.* Ag/AgCl). Nyquist diagrams were also recorded.

Chrono-amperometric measurements were conducted at −200 mV; a magnetic stirrer was used to provide the convective transport in 10 mL of 0.1 M phosphate buffer with 0.1 M KCl. Electrochemical experiments were carried out at room temperature.

Results and discussion

Morphological studies

Transmission electron micrographs of IrOx NPs were obtained to determine the particle sizes and homogeneity. Fig. 1A displays a typical TEM image of the synthesized IrOx nanoparticles (12.5 ± 2.5 nm) (see inset in Fig. 1A). Although the dispersion of these nanoparticles was not homogenous in the solution, most of the formed IrOx NPs exhibited spherical shape. These nanoparticles seem to be clusters of other smaller nanoparticles with diameters around 1.5 ± 0.3 nm.

The XPS spectra of IrOx NPs (Fig. S1†) showed the shifting of the Ir $4f_{7/2}$ and $4f_{5/2}$ peaks to ~62.3 and ~65.1 eV, and an increase of the O 1s peak intensity at 531.6 eV (main peak) and 533.7 eV (small peak), these results being in good agreement with the characteristics of a high oxidation state 4^+ of iridium.

IrOx NPs were immobilized onto an SPCE working electrode, then GA was used as cross-linking agent followed by modification with a solution composed of tyrosinase and BSA. The obtained biosensor was carefully characterized in each of the fabrication steps by using optical and electrochemical methods. Fig. 1B shows an SEM image of SPCE (left image corresponds to backscattered electrons mode). Fig. 1C displays the distribution of the IrOx NPs onto the working electrode surface of the SPCE. IrOx NPs appear brighter in the backscattered electrons image (Fig. 1C left), while the effect of glutaraldehyde as a binding matrix was more evident in normal mode (Fig. 1C right). An enhancement of the contrast between objects of different chemical compositions using backscattered electrons mode is observed, since heavy elements backscatter electrons more strongly than light elements. Finally Fig. 1D shows a good entrapment of the IrOx NPs, glutaraldehyde and tyrosinase–BSA.

To study the surface features of the modified electrodes, electrochemical impedances spectroscopy was used. The EIS curve presented as Nyquist plot consists of two parts: one part is the semicircle section, located at higher frequencies corresponding to the electron transfer limited process; the second part is related to the electron-transfer resistance (R_{ct}) and can be obtained by measuring its diameter. Another important part of the Nyquist plot is the linear section, which provides information related to the diffusion process held in solution and located at lower frequencies. The increase of electron transference due to the presence of the IrOx NP layer was observed with the decreasing of R_{ct} in the Nyquist plot (see Fig. 1E). These improvements were due to the fact that IrOx is a metallic oxide known for its high conductivity that corresponds to the high oxidation state (4^+) of iridium.[27,30] Additionally, this nanostructured platform based on IrOx NPs has a high surface area that contributes to the conductivity improvement.

The adsorption of glutaraldehyde onto the IrOx (see R_{ct} increase in Fig. 1E) indicates the effect of glutaraldehyde as a good binding/entrapment matrix. Finally, when the solution composed of Tyr–BSA was introduced (adsorbed onto the

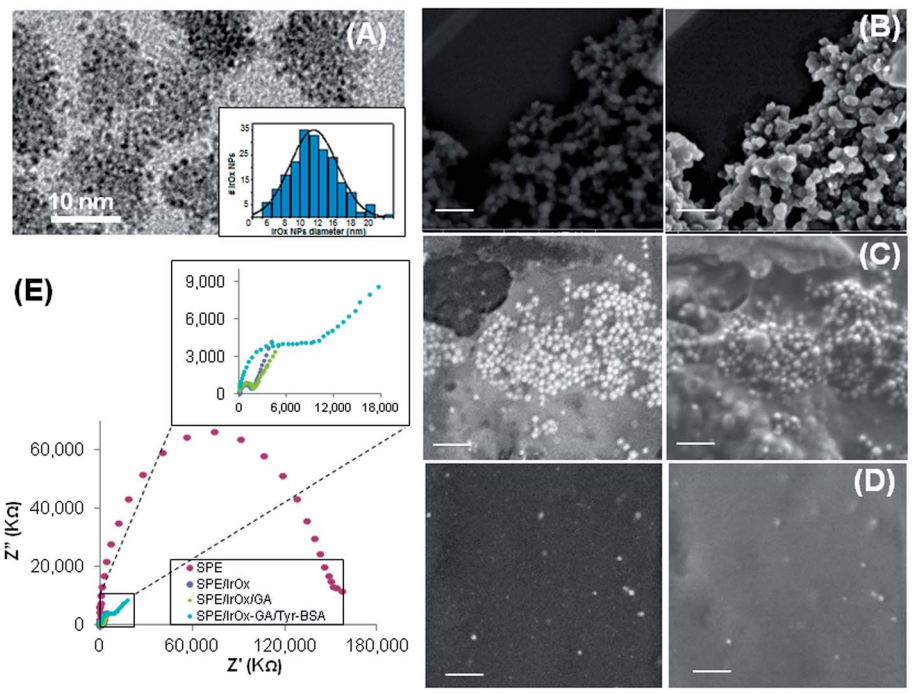

Fig. 1 Surface characterization. (A) TEM images of IrOx NPs. SEM images of SPCE (B), SPCE/IrOx/GA (C) and SPCE/IrOx/GA/IrOx–BSA (D). Impedance studies (E) of the modified electrodes surfaces. Left SEM images were taken using backscattered electrons mode. The scale bar of SEM images is 200 nm.

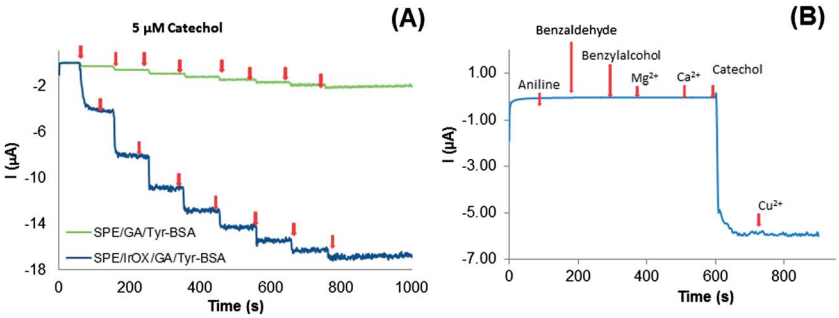

Fig. 2 Current–time responses of SPCE/GA/Tyr–BSA and SPCE/IrOx/GA/Tyr–BSA for the successive addition of 5 μM catechol solution, during stirring within a working potential of −0.2 V using 0.1 M phosphate buffer (PB) at pH 6.5 with 0.1 M KCl (A). Selectivity evaluation for catechol biosensor in the presence of successive additions of 50 μM aniline, benzaldehyde, benzyl alcohol, Mg^{2+}, Ca^{2+}, 5 μM catechol and 25 μM Cu^{2+} (B).

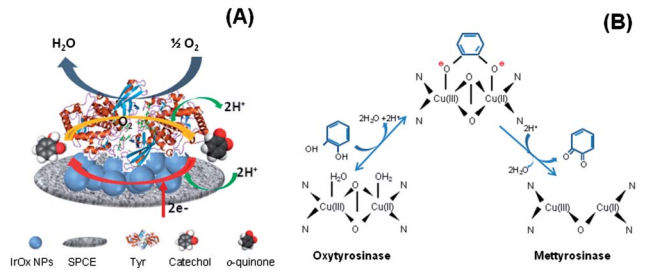

Fig. 3 Schematic representation of proposed detection mechanism, displaying the tyrosinase (Tyr) and reaction involved in the catechol detection at the SPCE modified with IrOx NPs (A). Catalytic cycles of the oxidation of catechol to *o*-quinone over two Cu atoms within the active site of tyrosinase enzymes (B).

electrode surface) an increase of R_{ct} as a result of the successful immobilization of the enzyme could be observed (Fig. 1E).

The SPCE/IrOx/Tyr biosensor operation for the catechol detection was evaluated by chrono-amperometric responses for the different enzyme modified sensors upon successive addition of 5 μM catechol (Fig. 2). This biosensor showed a higher current change in comparison to SPCE/Tyr (Fig. 2A). The observed reduction of the current was attributed to the direct reduction of *o*-quinone to catechol, released from the enzyme-catalyzed reaction on the electrode surface (see Fig. 3A and B). Tyrosinase has oxidase activity for oxidation of catechol to *o*-quinone (see Fig. 3B). At moderate negative potentials the *o*-quinone product of phenol oxidation may be electrochemically reduced to catechol (Fig. 2A). Oxidation by the enzyme followed by reduction at the electrode may result in cycling between the catechol and *o*-quinone.[18]

Fig. 2B shows a good selectivity of this biosensor toward catechol detection that is evident by the shown negligible responses toward interfering species. The chrono-amperometric responses toward aniline, benzaldehyde, benzyl alcohol, Mg^{2+}, Ca^{2+} (each one at a concentration 10 times higher than the phenol concentration) and Cu^{2+} (5 times higher than the phenol concentration) were measured. The selected species for interference studies seem to be the ones usually present with phenolic compounds in contaminated samples.[18]

Analytical characterization of the biosensor

The chrono-amperometric response of the SPCE/IrOx/Tyr biosensor to successive additions of catechol solution (Fig. 4A) was further evaluated under optimized experimental conditions (data not shown). A linear biosensor response within the range from 0.25–27.5 μM catechol with $r = 0.99$ was observed. The biosensor shows sensitive bioelectrocatalytic response, reaching about 95% of the steady-state current within 10 s after each addition of catechol.

The typical calibration curve of the SPCE/IrOx/Tyr biosensor for catechol is shown in Fig. 4B. Moreover, LOD and LOQ were calculated according to the 3 times *s*/*m* and 10 times *s*/*m* criteria, respectively, where '*s*' is the standard deviation of the peak

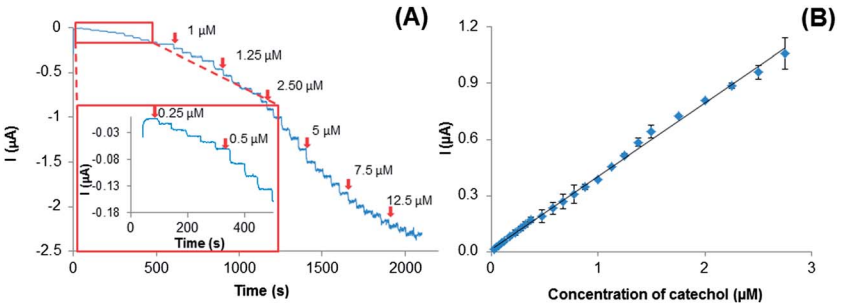

Fig. 4 Typical current–time response curves for the successive additions of different catechol concentrations (A); inset: magnification of the initial steps. Biosensor calibration given as current *versus* catechol concentration (B).

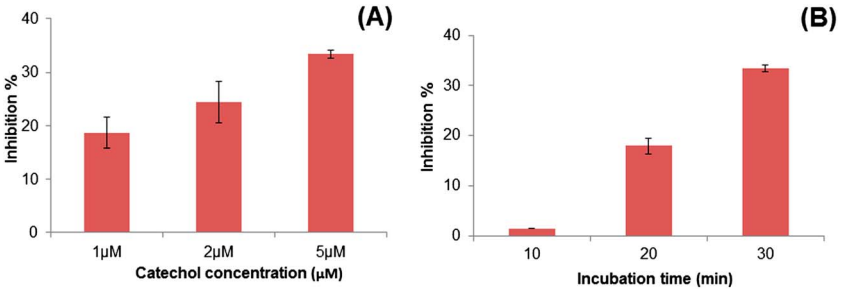

Fig. 5 Effects of substrate amount (A) and incubation time (B) on the residual activity of the catechol biosensor after pesticide incubation.

current of low concentration of the analyte (five runs) and 'm' is the slope of the related calibration graph.[31–35] The SPCE/IrOx/Tyr biosensor shows LOD = 0.08 μM and LOQ = 0.24 μM for catechol. The results of triplicate sets indicated by error bars reveal the in-day repeatability (Fig. 4B) of the measurements with a relative standard deviation (RSD) lower than 10%. Between-day repeatability was also obtained with a RSD value lower than 15%.

Pesticides are known to inhibit different enzymatic systems, tyrosinase being one of these.[15] To evaluate pesticide inhibition activity on the tyrosinase biosensor, the 'percentage inhibition' method was followed. The Tyr biosensor was immersed into a buffer solution under stirring and addition of catechol 5 μM was performed waiting until a steady state current response was achieved.

The stationary state current after each addition (I_{ss}) is related to the enzyme activity of the biosensor when the inhibitor is not present. After that the same biosensor was incubated during a fixed interval of time (30 min) with chlorpyrifos pesticide. The pesticide incubated biosensor was measured again after the addition of the same concentration of catechol (5 μM). Lower steady-state currents (I_p) were obtained due to inhibition by the pesticide. The Tyr biosensor inhibition percentage is calculated using the following equation:

$$I(\%) = \left[\left(I_{ss} - I_p\right)/I_{ss}\right] \times 100 \quad (1)$$

In order to optimize the testing variables for pesticide detection using tyrosinase inhibition, catechol concentration and incubation time were evaluated in the presence of 0.1 μM chlorpyrifos. Fig. 5A shows the optimum catechol concentration value to be used as the working substrate for Tyr inhibition experiments. Herein different concentrations of catechol (1, 2 and 5 μM) were used, and the best inhibition response was found to be achieved for a 5 μM substrate solution. The incubation time was also evaluated (see Fig. 5B) showing that when the incubation time increased the inhibition also increased. A 30 min incubation time (with stirring at 37.5 °C) was used for the following experiments.

A plot of the biosensor inhibition percentage as a function of pesticide concentration is shown in Fig. 6A. The proposed biosensor provides a linear range for chlorpyrifos concentrations from 0.01 to 0.1 μM with a correlation coefficient of 0.99 with a LOD = 0.003 μM and LOQ = 0.010 μM. As the pesticide irreversibly inhibits the enzyme, a new biosensor has to be used for each point of the calibration after being exposed to the pesticide. The results indicated by error bars reveal the in-day repeatability (Fig. 6A) of the measurements with a relative standard deviation (RSD) lower than 15%. Between-days repeatability was also obtained with a RSD value lower than 15%. These biosensors for CFP detection present high analytical performances in terms of sensitivity and LOD (Table 1 in ESI†).

To further demonstrate the applicability of the proposed biosensor, recovery tests by adding chlorpyrifos 0.1 μM into river and tap water were also performed. The results are presented in Fig. 6B. Recovery percentages of 113% ± 3.6 and 90%

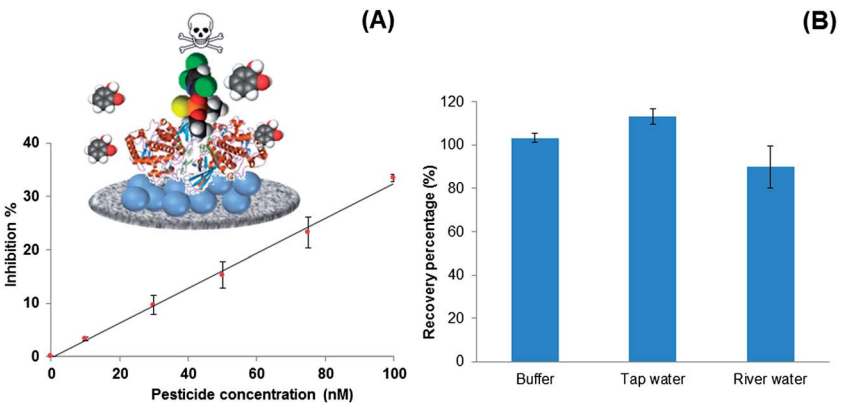

Fig. 6 Calibration curve of the biosensor as a function of the CPF concentration and the inhibition percentage (A). CPF recovery percentage from PBS, tap water and river water, using catechol biosensor (B).

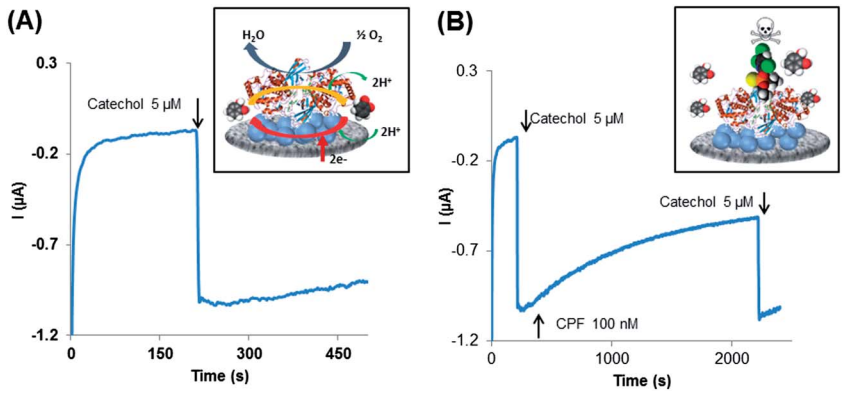

Fig. 7 IrOx nanoparticle induced dual catalytic/inhibition based detection of catechol (A) and CPF (B) using the same platform.

± 9.6 for tap and river water respectively with RSD lower than 10% ($n = 3$) were found. Recovery percentages were calculated using eqn (2).

$$\text{recovery percentage} = \left(\frac{[\text{CPF}]_{\text{buffer}}}{[\text{CPF}]_{\text{real sample}}}\right) \times 100 \qquad (2)$$

This indicates that the proposed biosensor can be used for trace level pesticide detection in real samples. In addition it is possible to detect catechol and CPF using the same platform given the fact that the catechol detection is almost instantaneous (10 s response time) and CPF detection requires a longer response (30 min) (see Fig. 7). It also can be extended to other kinds of enzyme and pollutant detection with interest for environmental monitoring.

Conclusions

An IrOx NP based biosensing platform with effective tyrosinase immobilization properties and corresponding catalytic effect toward catechol is developed. Due to the high conductivity and the surface active area of the IrOx NPs, the proposed biosensor displays dramatic improvements of the analytical performance in terms of a wide linear range of response along with a good LOD and sensitivity for catechol detection. Moreover the chlorpyrifos pesticide is detected using the same biosensor through the enzyme inhibition mechanism. The LOD was found to be 0.003 μM which is lower than the maximum contaminant level recommended by the European Environment Bureau.[36] In addition to the analytical performance the use of this biosensor for chlorpyrifos detection has advantages in comparison to other ones reported previously (Table 1 in ESI†) due to the fact that it is based on a simple cost-efficient screen-printed carbon electrode. In addition it is possible to detect catechol and CPF using the same platform. A careful operation of this platform should be versatile and efficient enough for dual detection applications. This dual phenol/pesticide detection biosensing system can be extended to other enzymes and consequently to other pollutants combining direct (catalytic) and indirect (inhibition) detection in the same platform.

Acknowledgements

This work was supported by a grant from MICINN through MAT2011-25870 project. S. Kurbanoglu acknowledges Ankara University's BEYOD program.

Notes and references

1 G. Aragay, F. Pino and A. Merkoçi, *Chem. Rev.*, 2012, **112**, 5317–5338.
2 C. W. Heath, *Cancer*, 1997, **80**, 1887–1888.
3 M. E. Ridano, A. C. Racca, J. Flores-Martín, S. A. Camolotto, G. Magnarelli de Potas, S. Genti-Raimondi and G. M. Panzetta-Dutari, *Reprod. Toxicol.*, 2012, **33**, 331–338.
4 A. Bódalo, E. Gómez, A. M. Hidalgo, M. Gómez, M. D. Murcia and I. López, *Desalination*, 2009, **245**, 680–686.
5 S. Viswanathan, H. Radecka and J. Radecki, *Biosens. Bioelectron.*, 2009, **24**, 2772–2777.
6 W. Zhong, D. Wang and X. Xu, *J. Hazard. Mater.*, 2012, **217–218**, 286–292.
7 A. Vermeulen, K. Welvaert and J. Vercammen, *J. Chromatogr., A*, 2005, **1071**, 41–46.
8 J. Gundel and J. Angerer, *J. Chromatogr., Biomed. Appl.*, 2000, **738**, 47–55.
9 J. Sherma, *Anal. Chem.*, 1993, **65**, 40R–54R.
10 I. Valenzuela, R. Lorenzini, M. J. Redondo and G. Font, *J. Chromatogr., A*, 1999, **839**, 101–107.
11 H. Wang, J. Wang, C. Timchalk and Y. Lin, *Anal. Chem.*, 2008, **80**, 8477–8484.
12 D. Du, W. Chen, W. Zhang, D. Liu, H. Li and Y. Lin, *Biosens. Bioelectron.*, 2010, **25**, 1370–1375.
13 J. Gong, Z. Guan and D. Song, *Biosens. Bioelectron.*, 2013, **39**, 320–323.
14 F. Arduini, S. Guidone, A. Amine, G. Palleschi and D. Moscone, *Sens. Actuators, B*, 2013, **179**, 201–208.
15 T. Liu, M. Xu, H. Yin, S. Ai, X. Qu and S. Zong, *Microchim. Acta*, 2011, **175**, 129–135.
16 S. Solé, A. Merkoçi and S. Alegret, *Crit. Rev. Anal. Chem.*, 2003, **33**, 89–126.
17 Y. D. Tanimoto de Albuquerque and L. F. Ferreira, *Anal. Chim. Acta*, 2007, **596**, 210–221.

18 C. C. Mayorga-Martinez, M. Cadevall, M. Guix, J. Ros and A. Merkoçi, *Biosens. Bioelectron.*, 2013, **40**, 57–62.
19 B. Pérez-López and A. Merkoçi, *Adv. Funct. Mater.*, 2011, **21**, 255–260.
20 C. Zhai, X. Sun, W. Zhao, Z. Gong and X. Wang, *Biosens. Bioelectron.*, 2013, **42**, 124–130.
21 S. Andrescu, L. Barthelmebs and J. L. Marty, *Anal. Chim. Acta*, 2002, **464**, 171–180.
22 J. P. Hart and S. A. Wring, *TrAC, Trends Anal. Chem.*, 1997, **16**, 89–103.
23 L.-G. Zamifir, L. Rotariu and C. Bala, *Biosens. Bioelectron.*, 2011, **26**, 3692–3695.
24 Y. Lin, F. Lu and J. Wang, *Electroanalysis*, 2004, **16**, 145–149.
25 S. Taufik, N. A. T. Yusof, T. W. Tee and I. Ramli, *Int. J. Electrochem.*, 2011, **6**, 1880–1891.
26 E. Katz and I. Willner, *Angew. Chem., Int. Ed.*, 2004, **43**, 6042–6108.
27 C. C. Mayorga Martinez, R. E. Madrid and C. J. Felice, *Sens. Actuators, B*, 2008, **133**, 682–686.
28 J. Tang, D. Tang, R. Niessner and D. Knopp, *Anal. Bioanal. Chem.*, 2011, **400**, 2041–2051.
29 T. Kuwabara, E. Tomita, S. Sakita, D. Hasegawa, K. Sone and M. Yagi, *J. Phys. Chem. C*, 2008, **112**, 3774–3779.
30 R. Meyer, S. Cogan, T. Nguyen and R. Rauh, *IEEE Trans. Neural Syst. Rehabil. Eng.*, 2001, **9**, 2–11.
31 C. M. Riley and T. M. Rosanske, *Development and validation of analytical methods*, Elsevier, New York, 1996.
32 M. E. Swartz and I. S. Krull, *Analytical method development and validation*, Marcel Dekker, New York, 1997.
33 J. Ermer and M. JHMcB, *Method validation in pharmaceutical analysis*, Wiley VCH, Weinheim, 2005.
34 P. De Bièvre and H. Günzler, *Validation in chemical measurements*, Springer, Berlin, 2005.
35 S. A. Ozkan, *Electroanalytical Methods in Pharmaceutical Analysis and Their Validation*, HNB Publishing, New York, 2012.
36 Council Directive 98/83/EC 1998 on the quality of water intended for human consumption, *Official Journal of the European Communities*, http://eurlex.europa.eu/LexUriServ/LexUriServ.do?uri=OJ: L:1998:330:0032:0054:EN: PDF.